Desalination 298 (2012) 67–74

Contents lists available at SciVerse ScienceDirect

Desalination

journal homepage: www.elsevier.com/locate/desal

Preparation and characterization of novel chitosan composite nanofiltration membrane containing mesogenic units

Tao Mu, Yuehua Cong, Wei Wang, Baoyan Zhang *

Centre for Molecular Science and Engineering, Northeastern University, Shenyang 110819, China

ARTICLE INFO

Article history:
Received 4 January 2012
Received in revised form 18 April 2012
Accepted 25 April 2012
Available online 27 May 2012

Keywords:
Polysulfone
Chitosan
Mesogenic compound
Composite nanofiltration membrane

ABSTRACT

Conventional nanofiltration (NF) membranes had a relatively low flux. In this paper, two mesogenic compounds were grafted to chitosan in order to change the structure, hence the performance of the NF membrane. A series of novel composite NF membranes were prepared by over-coating the polysulfone ultrafiltration membrane with the mixture of chitosan and mesogenic compounds modified chitosan. The two mesogenic compounds and their chitosan derivatives were characterized by infrared spectrophotometer (IR), differential scanning calorimetry (DSC), polarized optical microscope (POM); the structure of the membrane was characterized by scanning electron microscopy (SEM). The composite NF membrane's rejection rate and flux were strictly related to the mesogenic compound grafted to chitosan and its composition. Extremely high flux, 2543.3 $lm^{-2} h^{-1}$ was observed with P_{2-4} composite NF membrane, and the rejection remained to be as high as 66.3% at 0.4 MPa with 1000 mg/L NaCl. These results, together with SEM and infrared images of the composite NF membrane, indicated that the mesogenic compound structure was crucial for the structure and function of the composite membrane.

© 2012 Elsevier B.V. All rights reserved.

1. Introduction

Nanofiltration (NF) membrane, a new type of separation membrane between reverse osmosis (RO) membrane and ultrafiltration (UF) membrane, has been actively developed in the recent years. Due to its high separation efficiency and low energy expenditure required in operation, NF has been applied alone or in combination with other separation process in many fields including water softening treatment of waste water, oil industry, food processing, etc. [1–3]. The major limitation of currently NF membrane is membrane fouling. A severe decline of flux over extended period of operation is the direct result. Many recent literature have reported different approaches to solve the problem [4]. High flux can be achieved by improving membrane preparation process or altering the membrane properties. This article is focusing on the latter approach to achieve high flux by adjusting the membrane hydrophobicity and surface charge. Chitosan, a cationic polysaccharide obtained by alkaline *N*-deacetylation of chitin, has been routinely used in membrane preparation due to its abundance, hydrophilicity and environmental benignancy. By hydroxylation and amination reactions, chitosan can be modified [5–10]. Employing chitosan and its modified derivatives, various NF membranes were reported by surface cross-linking, blending and ultraviolet irradiation preparation methods [7–11].

Composite NF membrane based on multi-layer composite structure was designed in this paper, with polysulfone UF membrane as the base to provide mechanical strength and the modified chitosan/chitosan mixture as the top layer to provide filtration function, aiming to achieve high rejection with high flux. As both rigid stripe structures and the helical structures existed in liquid crystal [12–16], two mesogenic compounds with such structures were grafted to chitosan through hydroxylation in this paper to provide the change of the structure, hence performance of the NF membrane [17–19]. A series of NF membrane were prepared with this design. The rejection rate of conventional chitosan nanofiltration membrane was about 40–60% for NaCl, in which flux was about 5–20 $lm^{-2} h^{-1}$ [20–22]. In this paper, the rejection of one particular NF membrane for NaCl solution was slightly higher than the reported value of nanofiltration membrane based on chitosan, more important the flux was about three orders of magnitude higher than other conventional chitosan nanofiltration membranes. This unique property, which has not yet been reported before, was believed to be the result of its structure at molecular level (i.e. the modification of chitosan with the right compositions). This result encourages further study of the structure–property relationship in future. In general, the novel NF membrane designed and prepared in this paper had high flux and low energy expenditure in operation, which potentially would have broad applications in different fields.

* Corresponding author at: Centre for Molecular Science and Engineering, Northeastern University, Shenyang 110819, Wenhua Road, Heping District, Shenyang City, Liaoning Province, China. Tel./fax: +86 24 83687446.
E-mail addresses: mutao780920@126.com (T. Mu), yuehuacong@hotmail.com (Y. Cong), hizklmn1234@163.com, baoyanzhang@hotmail.com (B. Zhang).

0011-9164/$ – see front matter © 2012 Elsevier B.V. All rights reserved.
doi:10.1016/j.desal.2012.04.028

2. Experimental

2.1. Materials and methods

A self-made test equipment was adopted for the membrane performance test, as shown in Fig. 1. DDS-307 conductivity meter (Shanghai Leici Instrument Factory) was used to evaluate the conductivity of solution; Spectrum One infrared spectrometer (PerkinElmer) was used to test the chemical composition of monomers and polymers; differential scanning calorimetry (DSC) analytical meter (NETZSCH DSC-204) was used for the measurement of thermal transition properties of monomers; Polarized Optical Microscopy (POM) (Leica) was used for the observation of the texture of monomers; SSX-550 type scanning electron microscope (Shimadzu) was used for the observation of the morphology of NF membrane; and Spotlight 300 infrared imaging system (PerkinElmer) was used to measure the distribution of the functional layer on the surface of the substrate layer.

Chitosan [Mw≥20,000 Da, degree of deacetylation (DD≥90%)]; 4-methoxybenzoic acid, N-methyl pyrrolidone and polyvinylpyrrolidone were all analytical grade purchased from Sinopharm Chemical Reagent Co. Ltd; hexanedioic acid, acetone, glutaraldehyde and polyvinyl alcohol were obtained from Shenyang Xinxi Reagent Factory; 4,4′-dihydroxybiphenyl was purchased from Beijing Chemical Plant; cholesterol was purchased from Henan Xiayi Bell Biological Products Co. Ltd; and polysulfone was purchased from Shanghai Shuguang Chemical Plastics Industrial Corporation.

2.2. Preparation of modified chitosan

The structure of mesogenic compound M_1, M_2 is shown in Figs. 2 and 3.

Chitosan was grafted polymerization with two monomers in different ratios. The polymerization schemes are shown in Figs. 4 and 5.

General procedure for mesogenic compounds modified chitosan preparation:

(1) M_1 and M_2 compound acid chloride derivatives were prepared by reacting M_1 and M_2 with $SOCl_2$ into at 50 °C for 6 h. The products were purified by distillation.
(2) The acyl chlorides obtained from last step were dissolved in chloroform and added to the chitosan methanesulfonic acid solution dropwise over 3.5 h. The ratio between chitosan and M_1, M_2 acyl chloride is listed in Table 1. Once the reaction was over, the reaction mixture was cooled down to 4 °C for 10 h before acetone precipitation treatment. The products were then filtered twice and allowed to dry under vacuum.

2.3. Preparation of UF membranes

The polysulfone UF membrane was prepared by phase inversion, process was as follows [23–26]:

(1) 4.2 g polysulfone was dissolved in 25.7 g N-methylpyrrolidone. To this solution 0.12 g acetone and 0.075 g polyvinylpyrrolidone (PVP) was added to form the casting solution, which was filtered through a G2 sand filter to remove the undissolved impurities. The solution was then deaerated by standing for 10 h.
(2) The casting solution was applied to a piece of gauze (80 hole) tiled on the glass. The solvent in the membrane was first partially evaporated at ambient temperature for a minute, then the membrane was transferred to a water bath to set.

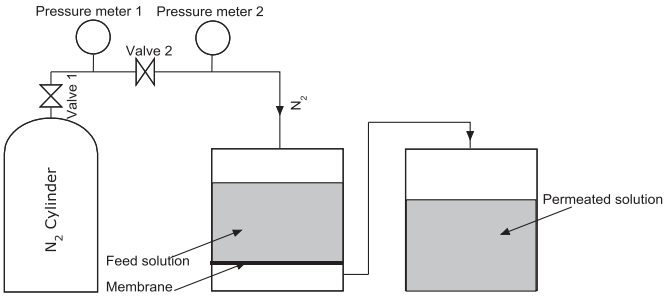

Fig. 1. Diagram of experimental apparatus for testing of the rejection and flux.

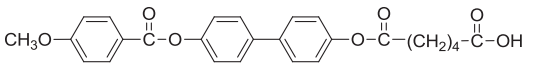

6-((4'-((4-methoxybenzoyl)oxy)-[1,1'-biphenyl]-4-yl)oxy)-6-oxohexanoic acid

Fig. 2. The structure of monomer M_1.

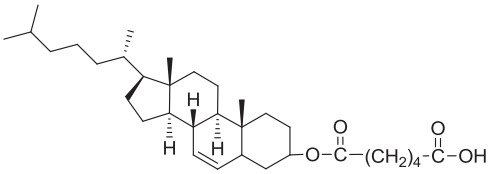

6-(((8*R*,9*R*,10*R*,13*S*,14*R*,17*S*)-10,13-dimethyl-17-((*S*)-6-methylheptan-2-yl)-2,3,4,5,8,9,10,11,12,13,14,15,16,17-tetradecahydro-1*H*-cyclopenta[*a*]phenanthren-3-yl)oxy)-6-oxohexanoic acid

Fig. 3. The structure of monomer M_2.

2.4. Preparation of composite NF membranes [27–31]

(1) The mixture of mesogenic compound modified chitosan and chitosan was dissolved in 2.5 ml 4% acetic acid solution with 0.04% polyvinyl alcohol (porogen). The casting solution was obtained by deaerating the above solution.
(2) The polysulfone UF membrane was fixed on the glass. The casting solution was then applied to coat the UF membrane. The newly formed membrane was vaporized for 60 s at room temperature, then cross-linked by 1% glutaraldehyde. The composite membrane was ready after 16 h at ambient temperature.

2.5. Permeation experiment

Flux and rejection were calculated based on the Eqs. (1) and (2).

$$F = V/At \quad (1)$$

where: F is the flux; V is the volume of the permeating fluid passing through the membrane; A is the effective area of membrane (0.93 cm^2); and t is the time for permeation.

$$R = \left(1 - C_p/C_0\right) \times 100\% \quad (2)$$

where: R is the rejection; and C_p and C_0 are the concentrations of the permeated fluid and feed respectively.

The concentration was replaced by the conductivity of salt solutions because the 1000 mg/L NaCl solution was a very dilute solution in this study.

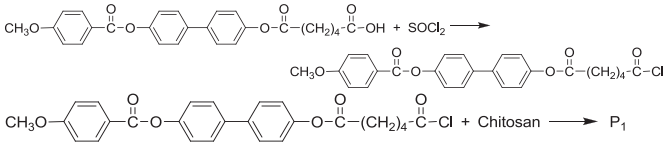

Fig. 4. Scheme of polymer P_1 synthesis.

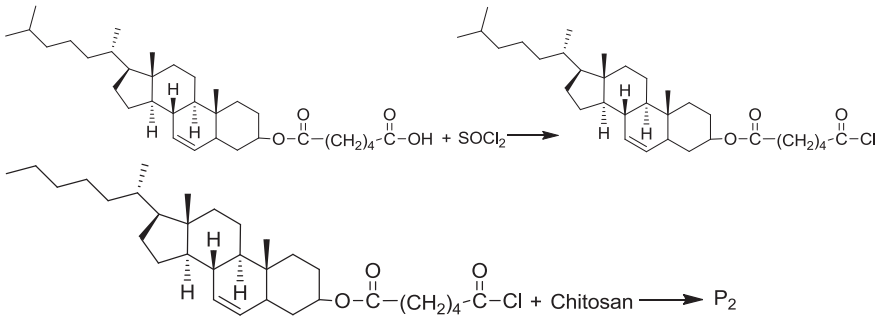

Fig. 5. Scheme of polymer P_2 synthesis.

3. Results and discussions

3.1. The characterization of the mesogenic compounds and the chitosan derivatives

3.1.1. Infrared analysis

Spectrum One infrared spectrometer was used to test the chemical compositions of the mesogenic compounds and the chitosan derivatives.

The infrared spectrum of M_1 is shown as Fig. 6. The absorption band at 3079 cm^{-1}–2854 cm^{-1} was associated with the stretching vibration of association hydroxyl of carboxylic acid; the absorption band at 1757 cm^{-1}–1700 cm^{-1} was associated with the stretching vibration of carbonyl; the absorption band at 1604 cm^{-1}–1493 cm^{-1} was associated with the stretching vibration of benzene; and the absorption band at 1257 cm^{-1}–1168 cm^{-1} was associated with the stretching vibration of ether linkage.

The infrared spectrum of M_2 is shown in Fig. 7. The absorption band at 3433 cm^{-1} was associated with the stretching vibration of hydroxyl of carboxylic acid; the absorption band at 2943 cm^{-1} and 2867 cm^{-1} was associated with the stretching vibration of the methyl and the methylene; and the absorption band at 1722 cm^{-1} and 1694 cm^{-1} was associated with the stretching vibration of carbonyl.

The infrared spectrums of polymers P_1 and P_2 are shown in Figs. 8 and 9. The conclusion could be drawn: comparing with the raw chitosan, the ester carbonyl absorption peak appeared at 1730 cm^{-1}, and the absorption peak of ester carbonyl increased with the ratio increase of monomer and primary hydroxyl of chitosan from bottom to top. M_1 and M_2 were successfully grafted to chitosan respectively.

3.1.2. Thermal analysis

The phase transitions and corresponding enthalpy changes of the mesogenic compound**s** were characterized by differential scanning calorimetry (DSC).

The DSC curve of monomer M_1 is shown in Fig. 10. The heating curve had two endothermic peaks, respectively, representing the melting transition (Tm = 187 °C) and the clearing transition (Ti = 361 °C), the endothermic enthalpy of which were ΔHm = 98.23 J/g and ΔHi = 2.46 J/g.

The DSC curve of monomer M_2 is shown in Fig. 11. The heating curve had two endothermic peaks, respectively, representing the melting transition (Tm = 137 °C) and the clearing transition (Ti = 147 °C), the endothermic enthalpy of which were ΔHm = 72.37 J/g and ΔHi = 1.15 J/g.

3.1.3. Textures analysis

The optical textures of the mesogenic compounds were studied by the polarized optical microscope (POM) with a hot stage under a nitrogen atmosphere.

Table 1
Polymerization feeding.

Polymer	m_{cts}/g	m_{M1}/g	m_{M2}/g	B
P_{n-0}	1.09	0	0	0
P_{n-1}	1.09	0.022	0.026	0.01
P_{n-2}	1.09	0.045	0.051	0.02
P_{n-3}	1.09	0.112	0.129	0.05
P_{n-4}	1.09	0.224	0.257	0.1
P_{n-5}	1.09	0.448	0.514	0.2
P_{n-6}	1.09	1.120	1.258	0.5
P_{n-7}	1.09	1.792	2.056	0.8
P_{n-8}	1.09	2.240	2.57	1.0

Note: n = 1, 2 represent respectively M_1, M_2 as the monomer polymerized with chitosan; B: the molar ratio of primary hydroxyl and monomer.

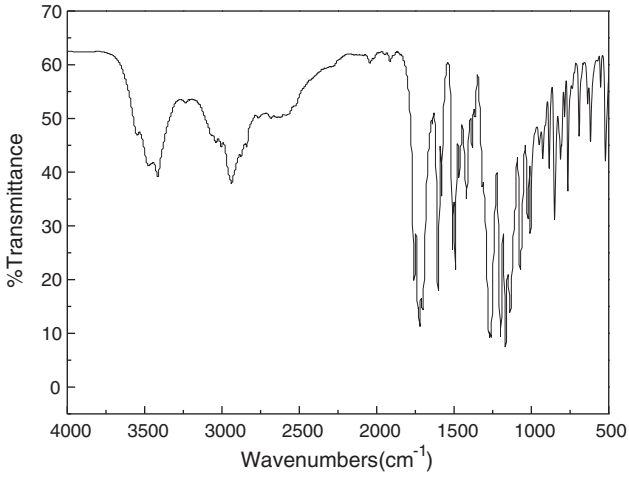

Fig. 6. IR spectrum of M_1.

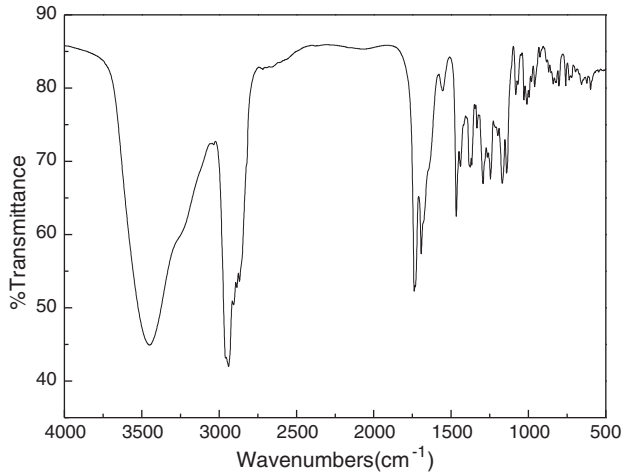

Fig. 7. IR spectrum of M_2.

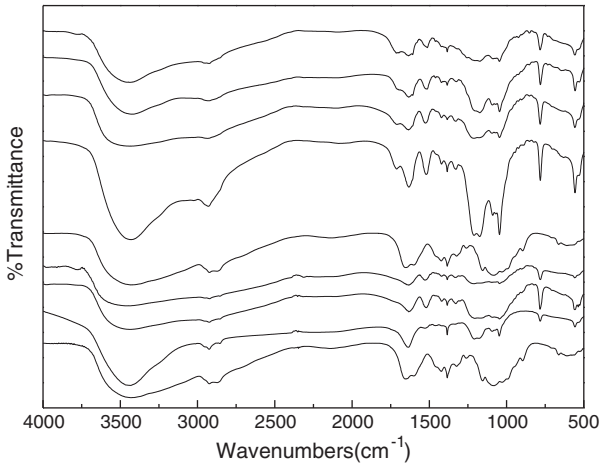

Fig. 8. IR spectrum of polymer P_1.

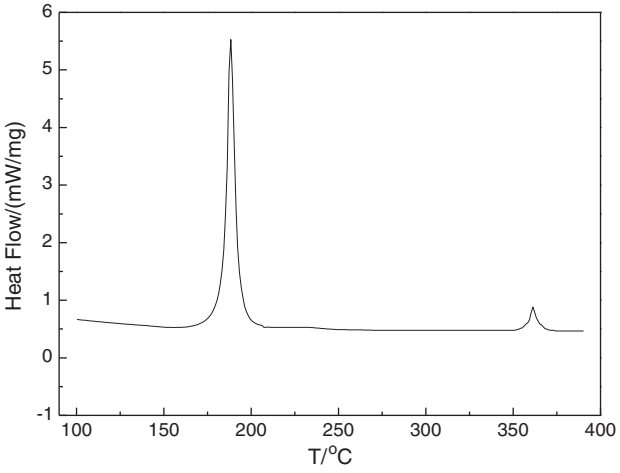

Fig. 10. Heating DSC curve of M_1.

The mesomorphism and textures of monomer M_1 are shown in Fig. 12. The visual observations under POM revealed that M_1 exhibited an enantiotropic schlieren texture and droplet texture during its heating and cooling cycles. When M_1 was heated to about 187 °C, it began to melt. At 305.9 °C, the schlieren texture of the nematic phase appeared as shown in Fig. 12(a), and the birefringence totally disappeared at 361 °C. When cooled to 238.9 °C from isotropic, the nematic droplet texture displayed, as shown in Fig. 12(b). The DSC and POM results indicated that M_1 was nematic thermotropic enantiotropic liquid crystal.

The mesomorphism and textures of monomer M_2 are shown in Fig. 13. The polarized optical micrograph of monomer M_2 revealed that M_2 exhibited an enantiotropic oily streak texture and a broken focal conic texture during its heating and cooling cycles. When M_2 was heated to about 137 °C, it began to melt. At 142.7 °C, the oily streak texture of the cholesteric phase appeared as shown in Fig. 13(a), and the birefringence totally disappeared at 147 °C. When cooled to 144.9 °C from isotropic, the broken focal conic texture was displayed, as shown in Fig. 13(b). It was typical cholesteric liquid crystal monomer.

The conclusion could be drawn from the analysis: M_1 and M_2 were grafted to chitosan respectively. M_1 was a nematic mesogenic compound with a rigid stripe structure; M_2 was a cholesteric mesogenic compound with a helical structure [14–16].

3.2. Effect of the degree of modified chitosan by different monomers on the rejection and flux of composite NF membrane

The test of two series of composite nanofiltration membrane was conducted after a pre-pressure at 0.4 MPa for 0.5 h. The relationships between grafting degree and membrane performance are shown in Figs. 14 and 15. The rejection of the nanofiltration membrane modified with mesogenic compound M_1 first increased and then decreased before it stabilized at a certain level with the increasing of M_1 grafting degree on the chitosan as shown in Fig. 14. In the case of the flux, it rose to 68,705 $lm^{-2}\,h^{-1}$ while the rejection was quite low, which was only 13.5%. This observation suggested M_1 modified chitosan and chitosan formed a large network structure. The rigid and bulk structure of M_1 caused the increased size of apertures comparing to chitosan alone. As a result the flux increased, while the rejection decreased. With mesogenic compound M_2, the rejection and flux both increased till 5% with P_{2-3} composite membrane. The rejection reached the maximum of 64.4% and corresponding flux was 2133 $lm^{-2}\,h^{-1}$ with P_{2-4} composite membrane when the grafting degree of M_2 to chitosan was 10%. When the grafting degree was higher than 10%, the rejection dropped and flux increased, indicating the filtration performance deteriorating. The data indicated the structure of M_2 and its appropriate composition in the chitosan derivative were crucial for the composite membrane performance. The reason may be as follows: with the right grafting degree, the helical structure of M_2 made the

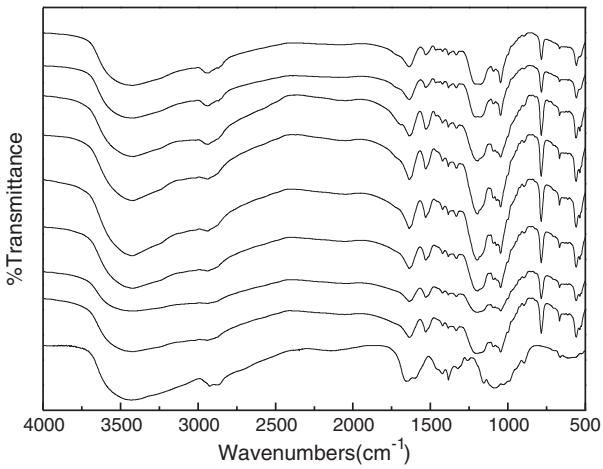

Fig. 9. IR spectrum of polymer P_2.

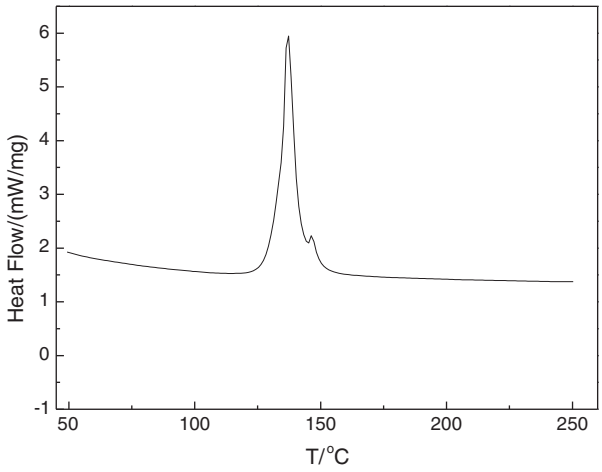

Fig. 11. Heating DSC curve of M_2.

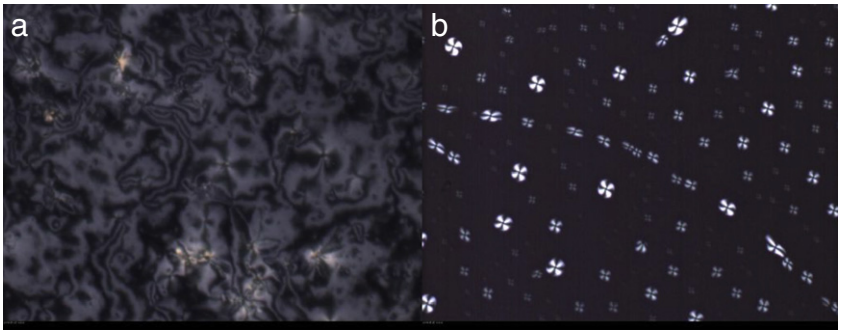

Fig. 12. Polarized optical micrograph of M_1.

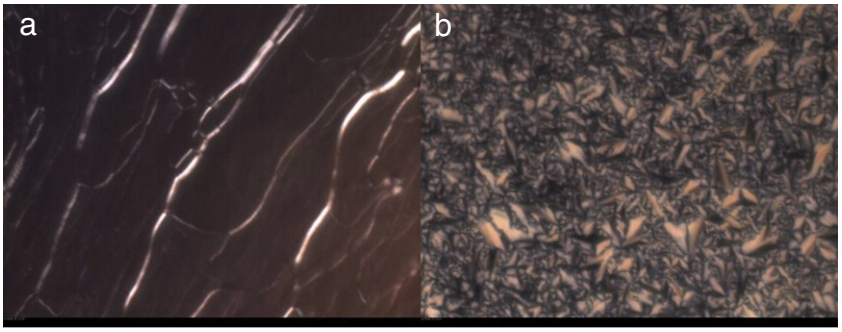

Fig. 13. Polarized optical micrograph of M_2.

tortuosity of the pore increase, while the pore became larger when the percentage of M_2 exceeded 10%, which might result from the bulk of M_2. Comparing with other conventional NF membrane, this membrane operated at low pressure with high flux [4,21,32,33], which had low energy expenditure and could be useful for water softening and the treatment of waste water. As the aim of the study was to obtain NF membrane with high rejection and high flux, P_{2-4} was selected as the casting material for further optimization.

3.3. Effect of the membrane preparation conditions on the performance of nanofiltration membrane

3.3.1. Effect of glutaraldehyde concentration on the rejection and the flux of composite NF membrane

The NF membranes were prepared with different concentrations of glutaraldehyde solution 0.1%, 0.2%, 0.5%, 0.75%, 1%, 1.25%, 1.5%, 1.75% and 2% as cross-linking agent. The effect of glutaraldehyde concentration on the performance of the composite membranes is shown in Fig. 16. The increase of the rejection with decrease of flux was observed as the concentration of glutaraldehyde increased from 0% to 1%. Once the concentration was higher than 1%, a sharp drop of rejection and a substantial increase of flux were the results. This phenomenon suggested at the beginning, that the cross-linking reaction occurred at the surface, which made the surface of membrane compact. When the glutaraldehyde concentration increased to 1%, the cross-linking reaction occurred in the entire active layer, which resulted in the formation of the larger network structure and increasing the size of pores buried in the active layer, thus the rejection decreased and the flux increased [21,34]. The maximum rejection was 64.4% with the flux as 2133 $lm^{-2}\,h^{-1}$ at the optimum concentration of the glutaraldehyde of 1%.

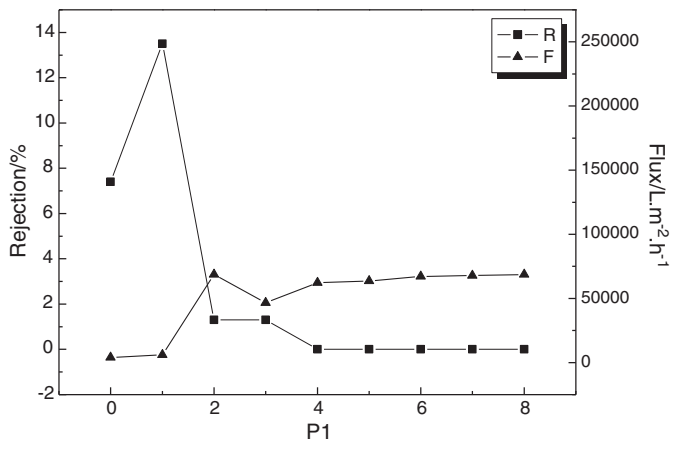

Fig. 14. Effect of the degree of the P_1 graft on the rejection and flux of the composite membrane.

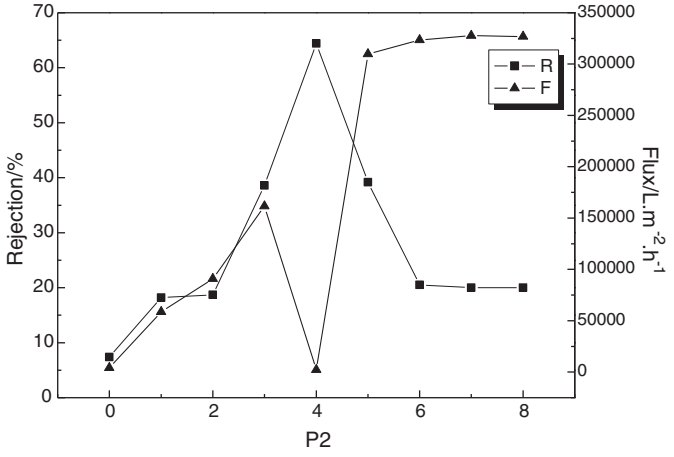

Fig. 15. Effect of the degree of the P_2 graft on the rejection and flux of the composite membrane.

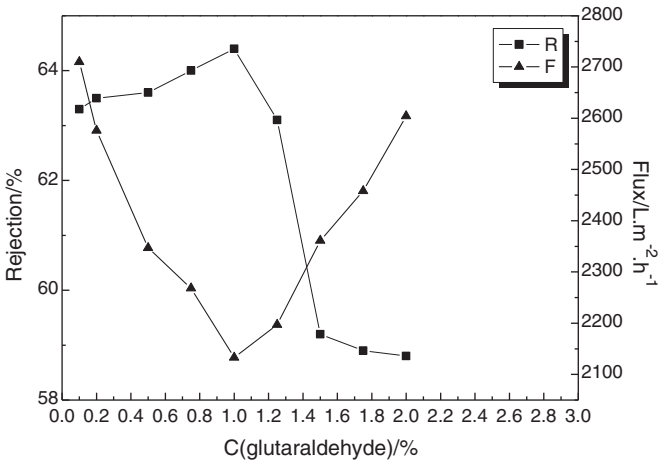

Fig. 16. Effect of glutaraldehyde concentration on the rejection and flux of composite membranes.

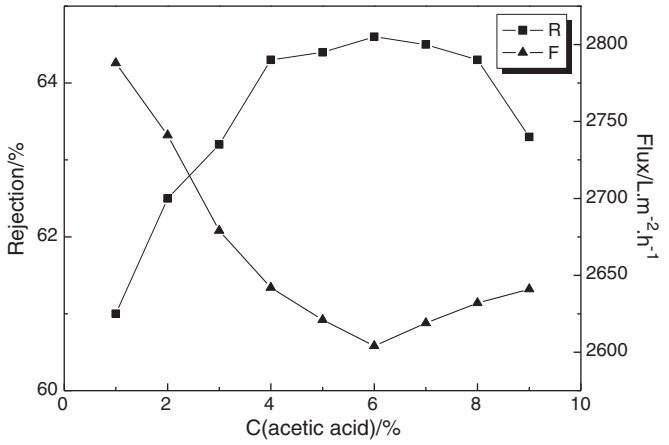

Fig. 18. Effect of acetic acid concentration on the rejection and flux of composite membrane.

3.3.2. Effect of polyvinyl alcohol concentration on the rejection and flux of composite NF membrane

The membranes were prepared with a range of concentrations of polyvinyl alcohol solution 0.01%, 0.02%, 0.04%, 0.06%, 0.08%, 0.1% and 0.12%. The effect of polyvinyl alcohol concentration on membrane rejection and flux is shown in Fig. 17. The impact of polyvinyl alcohol concentration on rejection was not very significant. With 0.06% of polyvinyl alcohol, the flux reached as high as 2642 $lm^{-2}\,h^{-1}$, while maintaining good rejection of 64.3%. Pore ratio increased along with the increase of the concentration, which led to enhanced flux with lessened rejection. However polyvinyl alcohol was not dissolved completely when its concentration exceeded 0.06%. Therefore, polyvinyl alcohol concentration 0.06% was selected.

3.3.3. Effect of acetic acid concentration on the rejection and flux of composite NF membrane

Different concentrations of acetic acid (1%, 2%, 3%, 4%, 5%, 6%, 7%, 8% and 9%) were used in the membrane preparation process. As illustrated in Fig. 18, the effect of acetic acid concentration on rejection and flux was in opposite trend as expected. With optimal concentration of acetic acid being 6%, both rejection (64.6%) and flux (2604 $lm^{-2}\,h^{-1}$) were high. Because chitosan was soluble in acetic acid but not in water, the chitosan was dissolved gradually along with the increase of the acetic acid concentration, which led to the forming of more compact film with decreased flux with increased rejection. When the acetic acid concentration reached to 6%, chitosan was dissolved completely. Higher concentration of acid might lead to the decomposition of chitosan's derivatives, which caused the porosity to increase. So the flux increased and rejection decreased instead.

3.3.4. Effect of cross-linking time on the rejection and flux of composite NF membrane

Cross-linking time influence on NF composite membrane function was also investigated. A series of membranes were prepared by cross-linking from 10 h up to 26 h with a 2-hour increase. Rejection and flux are shown in Fig. 19, the rejection increased firstly, then decreased before it stabilized at a certain level whereas the flux decreased firstly, then increased before it stabilized at a certain level. The maximum rejection was 65%, and the corresponding flux was 2602 $lm^{-2}\,h^{-1}$. Because the pore contraction and the tortuosity increased with prolonged cross-linking time, the increased rejection with the decrease of flux was observed. However when the cross-linking was longer than 14 h, the Schiff base might be decomposed, which was consistent with the literature [20,22]. Therefore, the optimal cross-linking time was 14 h.

3.3.5. Effect of ratio between P_{2-4} and the chitosan on the rejection and flux of composite NF membrane

A series of composite NF membranes were prepared with P_{2-4} and the chitosan at the ratio of 0:9, 1:8, 2:7, 3:6, 4:5, 5:4, 6:3, 7:2 and 8:1. As shown in Fig. 20, the rejection increased first, then decreased and the flux showed the opposite trend. Because the P_{2-4} was water

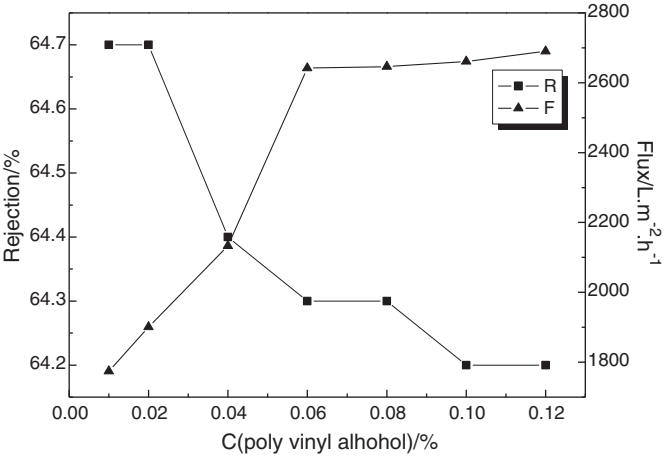

Fig. 17. Effect of polyvinyl alcohol concentration on the rejection and flux of composite membrane.

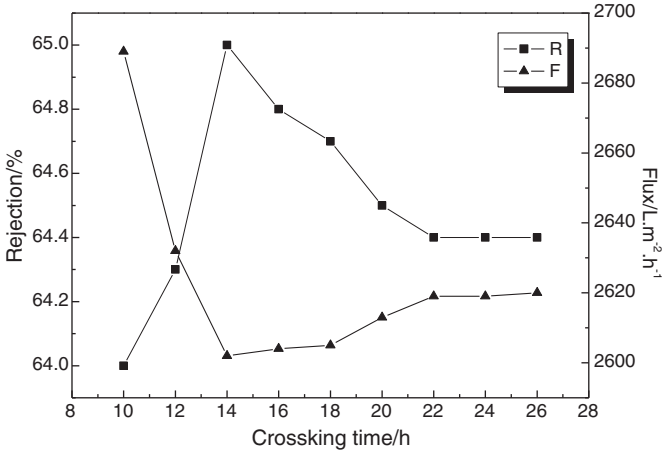

Fig. 19. Effect of cross-linking time on the rejection and flux of composite membrane.

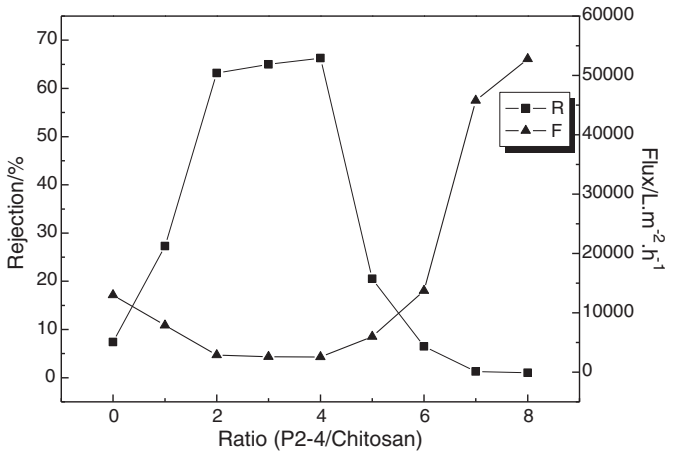

Fig. 20. Effect of ratio between P_{2-4} and the chitosan on the rejection and flux of composite membrane.

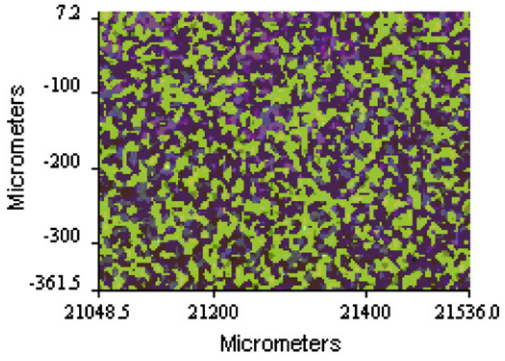

Fig. 22. Infrared imaging of composite membrane surface.

soluble with relative large volume, it might attach to the wall of pore at beginning. This led to the flux decline and the rejection increase. With the proportion of P_{2-4} increasing, it was hard to film on the basement membrane. The size of pore was at the level of ultrafiltration, so the flux increased and the rejection decreased. When the proportion of P_{2-4} increased continuously, it could not form a film on polysulfone surface. The phenomena of adsorption would no longer occur and the aperture size remained the same. The flux and rejection stabilized at the same level. Therefore, the optimal ratio was 4:5.

Based on the above results, the best experimental conditions of composite membrane preparation were as the following: glutaraldehyde concentration was 1%; polyvinyl alcohol concentration was 0.06%; acetic acid concentration was 6%; cross-linking time was 14 h at room temperature; and the ratio of P_{2-4} and the chitosan was 4:5. The rejection of compared NF membrane was 66.3%, the flux of which was 2543.3 $lm^{-2}\,h^{-1}$ with the 1000 mg/L of NaCl.

3.4. Structure characteristic of composite membrane

The cross-section and surface of this membrane were characterized by a SSX-550 scanning electron microscope as shown in Fig. 21. The composite membrane surface was magnified 30,000 times as shown in Fig. 21(a), and (b) was 1000 times magnification of the cross-section of the membrane. The surface of composite membrane was compact with some elevated area, which indicated that the surface was not completely smooth but with small gel particles in it. They formed the active layer of composite membrane. The cross-section of composite membrane had two layers. The upper was the thin and dense cross-linking layer; the lower was the polysulfone support layer with a sponge-like structure. The combination of the top dense function layer and the loose supporting layer allowed the composite membrane maintaining high rejection with high flux.

3.5. Infrared imaging analysis of composite membrane surface

The composite NF membrane was also analyzed using IR imaging technology. It is shown in Fig. 22, that the green zone represented the polysulfone membrane layer corresponding to the characteristic peak of 1252.50 cm^{-1}, the dark purple represented chitosan corresponding to the characteristic peak of 1653.88 cm^{-1}, and light purple represented modified chitosan, corresponding to the characteristic peaks to 1731.32 cm^{-1}. The modified chitosan and chitosan are distributed evenly on the surface of the polysulfone membrane.

4. Conclusions

The composite nanofiltration membrane reported in this paper was structured with two layers: the upper was the thin and dense cross-linked layer, which played a crucial role in separation; and the lower was the polysulfone support layer, with a sponge-like porous texture. The upper layer was prepared with a homogenous mixture of mesogenic compounds modified chitosan and chitosan. With the optimal composite membrane preparation conditions (1% glutaraldehyde concentration, 0.06% polyvinyl alcohol concentration, 6% acetic acid concentration, 14 h cross-linking time at room temperature, the ratio between P_{2-4} and the chitosan 4:5), the rejection of the membrane was 66.3% with flux as high as 2543.3 $lm^{-2}\,h^{-1}$ with the 1000 mg/L of NaCl at 0.4 MPa. This excellent high flux was the result of the membrane structure and function modification through the introduction of mesogenic compounds. These two compounds, M_1 and M_2, both had distinct structures. Increasing flux with relatively low rejection was observed with M_1 modified chitosan composite membrane due to the porous function layer caused by the introduction of M_1. The best performance was achieved with composite membrane with P_{2-4}. The unique structure of mesogenic compound M_2 allowed extra high flux with very good rejection. Further study of this unique membrane is ongoing. This work might open the possibility to improve NF membrane properties by introducing novel compounds.

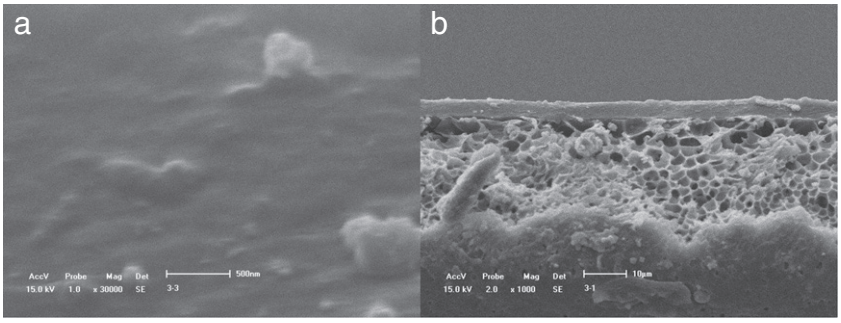

Fig. 21. The surface (a) and cross-section (b) images of the composite membrane.

Acknowledgments

Financial support from the National Key Technology Support Program of China (No. 2008BAL55B03) is gratefully acknowledged.

References

[1] A. Gao, Preparation and characterization of polypiperazine-amide composite nanofiltration membrane, Master Thesis, Zhengzhou University, 2002.
[2] C. Gao, Y. Chen, Nanofiltration membrane and its application, TNMSC 14 (2004) 310–316.
[3] Z. Wang, Fundamentals of Membrane Separation Technique, Chemical Industry Press, Beijing, 2000.
[4] K. Yoon, K. Kim, X.F. Wang, D.F. Fang, B.S. Hsiao, B. Chu, High flux ultrafiltration membranes based on electrospun nanofibrous PAN scaffolds and chitosan coating, Polymer 47 (2006) 2434–2441.
[5] L. Sun, J. Qi, H. Ge, Nanofiltration technology and applications, Chem. Equip. Technol. 25 (2004) 8–12.
[6] Y. Zhu, Preparation and optimization of chitosan composite nanofiltration membrane, Master Thesis, Ocean University of China, 2007.
[7] C. Xu, C. Lu, M. Ding, Synthesis and structure characterization of the quaternary ammonium salt of chitosan, J. Funct. Polym. 10 (1997) 51–55.
[8] R. Huang, G. Chen, J. Wang, Study on preparation and rejection performance of a novel kind of quaternary ammonium salt of chitosan/polyacrylonitrile composite nanofiltration membrane, Mod. Chem. Ind. 26 (2006) 204–208.
[9] R.-H. Huang, G.-H. Chen, M.-K. Sun, Y.-M. Hu, C.-J. Gao, Preparation and characteristics of quaternized chitosan/poly(acrylonitrile) composite nanofiltration membrane from epichlorohydrin cross-linking, Carbohydr. Polym. 70 (2007) 318–323.
[10] R. Huang, G. Chen, M. Sun, C. Gao, Preparation and characterization of quaterinized chitosan/poly(acrylonitrile) composite nanofiltration membrane from anhydride mixture cross-linking, Sep. Sci. Technol. 58 (2008) 393–399.
[11] C. Marconnet, A. Houari, D. Seyer, M. Djafer, G. Coriton, V. Heim, P. Di Martino, Membrane biofouling control by UV irradiation, Desalination 276 (2011) 75–81.
[12] Q. Zhou, X. Wang, Liquid Crystal Polymer, Science Press, Beijing, 1994.
[13] T. He, H. Hu, Functional Polymer and New Technology, Chemical Industry Press, Beijing, 2001.
[14] D. Wu, X. Xie, J. Xu, Polymer Liquid Crystals, Sichuan Education Publishing House, Chengdu, 1988.
[15] J. Lin, Fundamentals of Steroid Chemistry, Chemical Industry Press, Beijing, 1989.
[16] X. Ye, Stereochemistry, Peking University Press, Beijing, 1999.
[17] J.E. Bara, A.K. Kaminski, R.D. Noble, D.L. Gin, Influence of nanostructure on light gas separations in cross-linked lyotropic liquid crystal membranes, J. Membr. Sci. 288 (2007) 13–19.
[18] D.L. Gin, J.E. Bara, R.D. Noble, B.J. Elliott, Polymerized lyotropic liquid crystal assemblies for membrane applications (vol 29, pg 367, 2008), Macromol. Rapid Commun. 29 (2008) 682–683.
[19] Y.-H. Cong, W. Wang, M. Tian, F.-B. Meng, B.-Y. Zhang, Liquid-crystalline behaviours of novel chitosan derivates containing singular and cholesteryl groups, Liq. Cryst. 36 (2009) 455–460.
[20] R. Huang, G. Chen, M. Sun, C. Gao, A novel composite nanofiltration (NF) membrane prepared from graft copolymer of trimethylallyl ammonium chloride onto chitosan (GCTACC)/poly(acrylonitrile) (PAN) by epichlorohydrin cross-linking, Carbohydr. Res. 341 (2006) 2777–2784.
[21] J. Miao, G.H. Chen, C.J. Gao, A novel kind of amphoteric composite nanofiltration membrane prepared from sulfated chitosan (SCS), Desalination 181 (2005) 173–183.
[22] R. Huang, G. Chen, B. Yang, C. Gao, Positively charged composite nanofiltration membrane from quaternized chitosan by toluene diisocyanate cross-linking, Sep. Sci. Technol. 61 (2008) 424–429.
[23] M. Marcel, Basic Principles of Membrane Technology, Tsinghua University Press, Beijing, 1999.
[24] D.B. Mosqueda-Jimenez, R.M. Narbaitz, T. Matsuura, Manufacturing conditions of surface-modified membranes: effects on ultrafiltration performance, Sep. Sci. Technol. 37 (2004) 51–67.
[25] D.B. Mosqueda-Jimenez, R.M. Narbaitz, T. Matsuura, G. Chowdhury, G. Pleizier, J.P. Santerre, Influence of processing conditions on the properties of ultrafiltration membranes, J. Membr. Sci. 231 (2004) 209–224.
[26] Y. Ma, F. Shi, J. Ma, M. Wu, J. Zhang, C. Gao, Effect of PEG additive on the morphology and performance of polysulfone ultrafiltration membranes, Desalination 272 (2011) 51–58.
[27] H. Peng, J. Chen, Z. Zeng, Q. Gong, S. Dong, Preparation and characterization of composite membrane based PAN ultrafiltration membrane, J. Fuzhou Univ. 01 (2004) 93–97.
[28] Y. Song, F. Liu, C. Zhao, B. Sun, Preparation and characterization of the composite nanofiltration membrane, J. Beijing Univ. Chem. Technol. 3 (1999) 38–45.
[29] J.M. Yang, W.Y. Su, Preparation and characterization of chitosan hydrogel membrane for the permeation of 5-Fluorouracil, Mater. Sci. Eng. C Bio S 31 (2011) 1002–1009.
[30] J. Ma, N.A. Choudhury, Y. Sahai, R.G. Buchheit, A high performance direct borohydride fuel cell employing cross-linked chitosan membrane, J. Power. Sources 196 (2011) 8257–8264.
[31] A.G. Boricha, Z.V.P. Murthy, Preparation and performance of N,O-carboxymethyl chitosan-polyether sulfone composite nanofiltration membrane in the separation of nickel ions from aqueous solutions, J. Appl. Polym. Sci. 110 (2008) 3596–3605.
[32] M. Jahanshahi, A. Rahimpour, M. Peyravi, Developing thin film composite poly(piperazine-amide) and poly(vinyl-alcohol) nanofiltration membranes, Desalination 257 (2010) 129–136.
[33] R. Malaisamy, A. Talla-Nwafo, K.L. Jones, Polyelectrolyte modification of nanofiltration membrane for selective removal of monovalent anions, Sep. Sci. Technol. 77 (2011) 367–374.
[34] D.A. Musale, A. Kumar, Effects of surface crosslinking on sieving characteristics chitosan/poly(acrylonitrile) composite nanofiltration membranes, Sep. Sci. Technol. 21 (2000) 27–38.